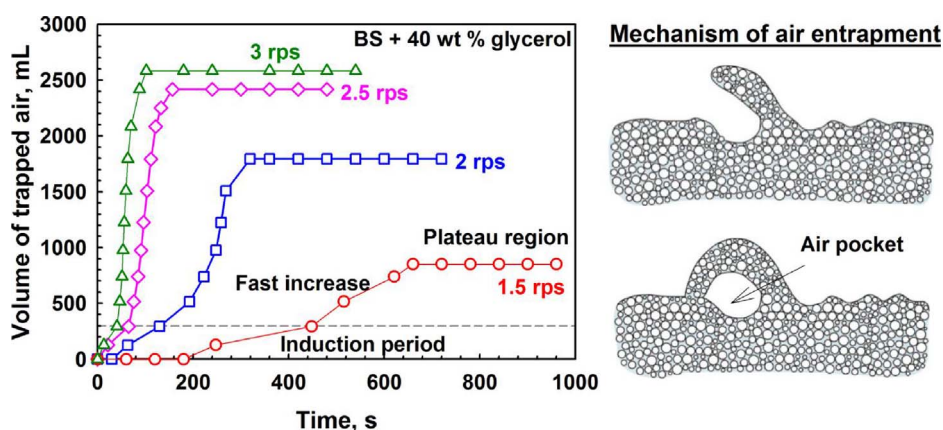# Self-regulation of foam volume and bubble size during foaming via shear mixing

Nadya Politova, Slavka Tcholakova*, Zhulieta Valkova, Konstantin Golemanov, Nikolai D. Denkov

Department of Chemical and Pharmaceutical Engineering, Faculty of Chemistry and Pharmacy, Sofia University, 1164 Sofia, Bulgaria

GRAPHICAL ABSTRACT

ARTICLE INFO

ABSTRACT

Here we study the factors affecting the foam generation in a planetary mixer with a series of surfactant solutions, having different dynamic surface tensions, surface dilatational moduli and bulk viscosities. The foam generation in this device consists of three well defined periods: (1) Induction period during which very slow increase of the foam volume is observed. The duration of this period depends significantly on the shear rate during foaming and on the volume of the surfactant solution; (2) Fast increase of foam volume; the rate of this process depends primarily on the shear rate and dynamic surface tension of the solutions; (3) Plateau region in which the foam volume remains constant. The experimental results show that the processes of air entrapment ends when a certain critical (dimensionless) shear stress of the foam is reached. Depending on the bulk and surface properties of the surfactant solutions, this critical stress is achieved for foams with different air volume fractions and mean bubble sizes. Thus, when solutions with higher bulk viscosity and/or higher surface modulus are used, the critical stress is reached at lower air volume fraction and with smaller bubbles. Power-law equations are shown to describe very well the effects of the foaming shear rate and solution viscosity on the final foam volume and mean bubble size.

* Corresponding author at: Department of Chemical and Pharmaceutical Engineering, Faculty of Chemistry and Pharmacy, Sofia University, 1 James Bourchier Ave 1164 Sofia, Bulgaria.
E-mail address: sc@lcpe.uni-sofia.bg (S. Tcholakova).

1. Introduction

Liquid foams find a variety of applications in everyday life and industry: as home and personal care products, and in cosmetics, firefighting, pharmaceuticals, enhanced oil recovery, etc. [1–3]. The foam properties and foam stability depend primarily on the air volume fraction in the generated foam, Φ, and the size distribution of the formed bubbles [1–8]. Depending on the foaming method, these two characteristics could be controlled separately or be interrelated. In the methods in which a given air volume is injected into the surfactant solution and the formed dispersion is stirred, the air volume fraction is pre-defined and the stirring conditions determine the size and the polydispersity of the formed bubbles only [9–12]. This regime of foam generation is studied in the literature and the main factors affecting the final bubble size distributions are determined experimentally and described theoretically [9–12].

On the other hand, in most every-day applications and in wide range of industrial processes, the foam generation consists of simultaneous processes of air entrapment and bubble breakage into smaller bubbles [1–4,13]. Various foaming methods are used in practice and in the scientific studies, aiming to characterize the foaming properties of the surfactant solutions in which both processes air entrapment and bubble breakage occur simultaneously. Typical examples for such methods are Ross-Miles test and Bartsch test [1–3,14–16]. In these methods the air entrapment occurs in a very short period of time during vigorous shaking in Bartsch method or falling of water jet in the Ross-Miles test. Due to the very short time in which the air entrapment occurs, the experimental results reported in the literature show that the foamability depends on the dynamic surface tension of the foaming solutions tested [17–27]. These two methods are inefficient for foam generation from viscous solutions which are often encountered in some applications, e.g. in food and some cosmetic systems [1–3].

For foaming of viscous solutions it is more appropriate to use mixers in which the shear forces act to ensure the simultaneous processes of air entrapment and bubble breakage. One of the widely used mixers of this type in the food, cosmetic and chemical industries is the planetary mixer [28,29]. The hydrodynamic conditions in the planetary mixers are very different as compared to the other types of foaming tests (Bickerman; Ross-Miles; Bartsch). In this method the foam is subjected to continuous deformation–a combination of shear and extension, which resembles the shearing of solutions for their mixing in various applications. The planetary mixer is particularly convenient to perform model experiments, aimed at understanding how the surface and bulk properties of the foaming solutions affect the process of foam formation, as one can study both the kinetics of foam generation and the properties of the final foam under well-defined conditions. Such a study is important not only from scientific but also from a practical viewpoint, as the optimal hydrodynamic conditions for foaming depend on the properties of the surfactant solution via a dependence which is not clear so far.

Therefore, the major aim of the current study is to investigate systematically the factors and mechanisms which control the process of foam generation under shear. The studied factors can be classified in two categories. The first category includes the material properties of the foaming solutions: (1) Viscosity; (2) Surface viscoelasticity; and (3) Dynamic surface tension, DST. The second category includes the external experimental conditions at which the foaming process is evaluated: (4) Rotation speed of the mixing tool which corresponds to different shear rates in the foamed solution, and (5) Volume of the foaming solution in the mixer container.

The focus of our study is on the role of the material properties of the foamed solutions, as well of the rotation speed of the mixing tool. We study the kinetics of the foam generation by monitoring the change of the volume of trapped air over time. The final foams, obtained at the end of the shearing process, are characterized in terms of their air volume fraction, average bubble size, and foam rheological properties. To obtain more detailed information about the mechanisms of air entrapment we performed also optical observations of the surface of the sheared foam with a high-speed video camera.

The article is organized as follows. The materials and methods are described in Section 2. Section 3 presents the main experimental results and their discussion. The conclusions from the study are summarized in Section 4.

2. Materials and methods

2.1. Materials

The experiments are performed with a mixture of the anionic surfactant sodium dodecyl-oxyethylene ether sulfate (SLES, commercial name STEOL-170, product of Stepan Co.) and the zwitterionic surfactant cocoamidopropyl betaine, CAPB (product of Goldschmith, commercial name Tego Betaine F50), containing different cosurfactants which are able to decrease the dynamic surface tension and to modify the dilatational surface modulus of the studied SLES + CAPB solutions. The mixture SLES + CAPB is denoted as BS (basic solution) in the text.

As cosurfactants we used a series of fatty acids and fatty alcohols with different chain-lengths. The fatty acids used are caprylic acid (C8Ac, product of Fluka), decanoic acid (C10Ac, product of Alfa Aesar) and myristic acid (C14Ac, product of Sigma-Aldrich). As fatty alcohols we used octanol (C8OH, product of Sigma-Aldrich) and decanol (C10OH, product of Sigma-Aldrich). The cosurfactant C14Ac leads to a surface dilatational modulus of the foamed solution (BS + C14Ac) which is two orders of magnitude higher, as compared to that of BS [30–32]. The shorter-chain fatty alcohols or fatty acids with 10 or less C-atoms in the chain (C8Ac, C8OH, C10Ac, C10OH) are used as cosurfactants which can decrease significantly the dynamic surface tension of the BS solution [32].

To vary in a systematic way the solution viscosity we added glycerol in different concentrations, from 30 to 90 wt.%. The glycerol was a product of Fluka (anhydrous p.a. 99.5% GC, Cat. No. 49770).

Initially we prepared concentrated surfactant solution of 10 wt% of SLES + CAPB (approx. 300 mM), at fixed weight ratio of 2:1, corresponding approx. to 200 mM SLES + 100 mM CAPB. The fatty acids and fatty alcohols were added at concentrations of 30 mM or 60 mM to the concentrated SLES + CAPB solution, upon stirring and heating up to 40 °C for C8Ac and C10Ac and up to 60 °C for C14Ac.

The solutions which were used in the actual foaming experiments were obtained from the concentrated stock solutions via 20-fold dilution with de-ionized water (Elix, Millipore). Thus, the concentration of the foamed BS solutions was 15 mM SLES + CAPB (2:1 by weight), with or without 1.5 mM or 3 mM cosurfactant.

2.2. Measurement of the dynamic and equilibrium surface tensions of the solutions

The equilibrium surface tension of the solutions was measured by Wilhelmy plate method on a tensiometer K100 (Kruss GmbH, Germany). The dynamic surface tension (DST) of the solutions was measured by the maximum bubble pressure method on tensiometer BP2 (Kruss GmbH, Germany) at 20 °C.

2.3. Measurement of the surface rheological properties of the solutions

The surface dilatational modulus was measured on DSA10 instrument (Kruss GmbH, Germany), equipped with Oscillating Drop Module (ODM module DS3260). The principle of the method and technical details are described in Ref. [33]. The experiments were performed at oscillation periods of 5 s (0.2 Hz). The amplitude of oscillation varied between 0.4 and 2.1%.
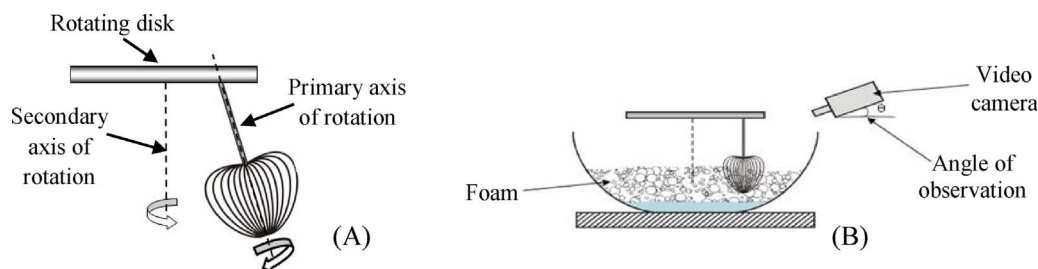
Fig. 1. Experimental set-up for monitoring the kinetics of foam generation. (A) Mixing tool in a planetary mixer; (B) Vessel containing the foamed solution (see also Supplementary Materials section). The surface of the solution or of the foam formed is observed with a high-speed video camera.

2.4. Measurement of the solutions' viscosity

The viscosity of the surfactant solutions were measured at 20 °C with capillary viscometer, after calibration with pure water. The density of the solutions was measured with DMA 35 Portable Density Metter (Anton Paar).

2.5. Procedure for foam generation in Kenwood Planetary mixer

To study the process of foam generation we used a planetary mixer Kenwood Chef Premier KMC 560 (1000 W). In this device, the mixing tool rotates simultaneously around two axes, see Fig. 1. The primary axis of rotation is the axis of the mixing tool. The second axis of rotation is located at the centre of the vessel which contains the foamed solution. Due to the similarity of this combined two-axial rotation to the motion of the Earth, which revolves around the Sun and around its own axis of rotation, this type of mixers is called "planetary mixer".

The geometrical parameters of the used mixer are described in a Supplementary Materials section. From these parameters we calculated the maximum shear rate in the mixer, which is realized in the gap between the rotating whisk and the internal wall of the foaming container. As explained in Supplementary Materials, all main effects discussed below occur in the mixer zone, in which the maximum shear rate is almost constant at a given rotation speed of the mixing tool. Therefore, there is a direct relation between the rotation speed of the mixer and the maximum shear rate in the bowl, at which the foaming process is realized.

In our experiments the surfactant solution with volume, V_0, was placed in a transparent vessel with total volume of 3250 mL. The mixing tool was rotated with a speed, expressed as rotations per second (rps). The relation between the rotation speed of the tool and the respective shear rate in the mixed system is given in Ref. [29] and according to this model the calculated shear rates in our experiments varied between 1.5 and 3 rps, which corresponds to 45–90 s^{-1}, respectively.

The experiments always started at the lowest rotation speed of 1.5 rps. If there was no any air entrapment for 10 min at this speed, the rotation speed was increased step-wise to the next one, 2 rps. These steps were repeated until we observed air entrapment at a given speed. The volume of the generated foam was monitored as a function of time. After a certain period of time the foam volume remained constant. To be sure that the maximum foam volume at the respective conditions is reached, we continued the foam shearing for at least 5 min after the foam volume stopped increasing. The foams obtained at the end of the shearing cycle were characterized in terms of their average bubble size and air volume fraction. We measured also the foam rheological properties under steady shear as explained in Section 2.8.

2.6. Optical observation of the process of air entrapment

We performed optical observations of the process of foam generation via high-speed video camera MotionXtra N3 (Redlake). The optical magnification was selected in such a manner, as to allow the observation of the deformation and flow of the foam at a macroscopic scale,

without being able to observe the individual small bubbles in a mesoscopic scale. Video records were made at different magnifications, frames per second (fps) and observation angles (θ), see Fig. 1.

2.7. Determination of the bubble size distribution and the average bubble size

Bubble size distribution in the final foams was determined by the method of Garrett et al. [34,35]. The foam was spread in a small petri dish and an optical triangular prism was placed on top, in direct contact with the foam. The foam was illuminated by diffuse white light through one of the prism side-walls, whereas the foam observation was made by video-camera, through the other side-wall of the prism. In the recorded images one sees the wetting films, formed between the bubbles and the prism wall, as bright polygonal spots, whereas the Plateau borders around the films are seen as dark interconnected areas. The foam images were processed via an open software package Image J, released by the National Institute of Health (NIH) [36]. For scaling the rheological data, the mean surface-volume radius, R_{32}, was used:

$$R_{32} = \sum_i R_i^3 \Big/ \sum_i R_i^2 \tag{1}$$

where the sum is taken over all measured bubbles in a given sample.

2.8. Characterization of foam rheological properties

The rheological properties of the studied foams were studied with rotational rheometer Bohlin Gemini (Malvern Instruments, UK). Parallel-plates geometry was used with 20 mm radius of the plates and 3 mm gap. On both plates we glued sand paper (P100) to suppress the foam-wall slip. Indeed, experiments performed with different gaps between the plates confirmed that the foam-wall slip was negligible. Rheological tests in steady shear deformation were performed. During the experiment, the shear rate, $\dot{\gamma}$, was varied logarithmically from 0.01 s^{-1} to 200 s^{-1} and the shear stress was recorded, $\tau = \tau(\dot{\gamma})$. The temperature was fixed at 20 °C. The procedure for interpretation of the experimental data obtained with Herschel-Bulkley fluids, such as the studied foams, is described in Ref. [37].

3. Experimental results and discussion

In Section 3.1 we present experimental results about the surface properties of the solutions studied. In Section 3.2 we describe results about the effect of the operating conditions on the foaminess of BS solution. The effects on foaming of the short-chain additives and glycerol are described in Sections 3.3 and 3.4, respectively. The optical observations of the foaming process and the observed mechanism which controls the final air volume fraction and the mean bubble size are presented Section 3.5. All results are discussed in a common framework in Section 3.6.

3.1. Surface properties of the solutions

To analyse the role of the surface properties on the foaming process we characterized: (1) the kinetics of surfactant adsorption by measuring
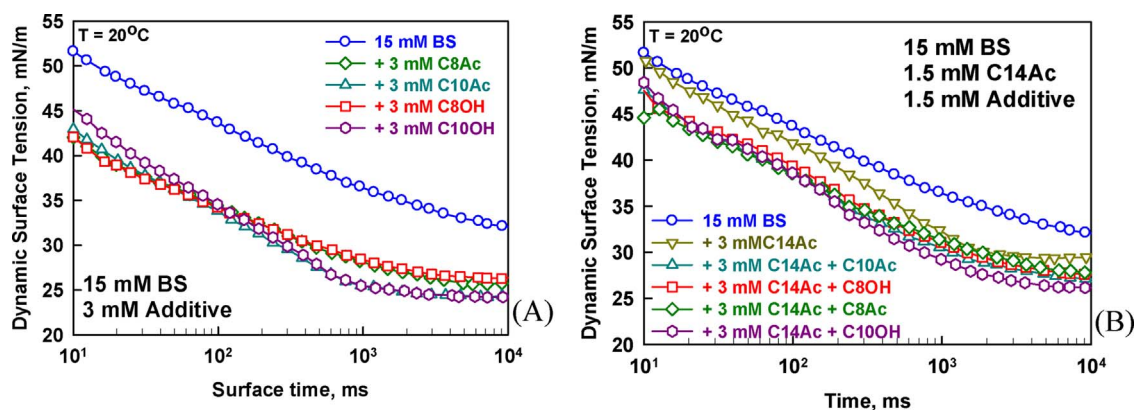
Fig. 2. Dynamic surface tesnsion vs. surface age of solutions of (A) BS + Additive; (B) BS + C14Ac + additive. Solutions: BS (blue empty stars); BS + C14Ac (black stars). The used additives are: C8Ac (red squares); C8OH (cyan triangles); C10Ac (green diamonds); C10OH (pink hexagons). (For interpretation of the references to colour in this figure legend, the reader is referred to the web version of this article.)

the dynamic surface tension, DST, and (2) the surface rheological properties by the oscillating drop method (ODM).

The obtained results for DST are shown in Fig. 2. From the data shown in Fig. 2A one sees that both the short-chain fatty acids and short-chain fatty alcohols decrease significantly the DST of the BS solution. In our previous study [32] we observed this effect with fatty acids and explained it with the structural perturbation of the mixed micelles of the main surfactants, SLES + CAPB, when short-chain cosurfactant molecules are solubilized in the micelles. As a result of this perturbation, the main surfactant molecules exchange more rapidly with the aqueous solution which accelerates their adsorption on solution surface. In the current study we show that similar perturbation of the micelles is induced by the short-chain alcohols, C8OH and C10OH.

The effect of the short-chain cosurfactants on the surface properties of BS + C14Ac solutions is illustrated in Fig. 2B. In these systems significant effect is observed at short time-scale mostly, whereas at longer time-scale there is a small difference between the surface tension of BS + C14Ac and BS + C14Ac + cosurfactant solutions, because condensed mixed adsorption layers are formed in the presence of C14Ac which are characterized with low equilibrium surface tension.

As shown in our previous studies [30–32], the addition of long-chain fatty acids, such as C14Ac, increases significantly the surface modulus of BS solutions, due to the formation of mixed adsorption layer on the solution surface which behaves as condensed surface layer with high viscoelasticity. On the other hand, the shorter-chain fatty acids are unable to induce such condensation of the adsorption layer [32]. For the current study we studied the effect of the short-chain (C8 and C10) fatty acids and fatty alcohols on the surface rheological properties of BS and BS + C14Ac solutions.

The obtained results show that the addition of short-chain fatty additives into BS and BS + C14Ac solutions leads to a decrease in the measured surface moduli, see Fig. 3. This effect is rather significant for BS + C14Ac solutions, as the additives decrease the surface modulus from ca. 300 mN/m down to ca. 100 mN/m. The lower surface modulus of the system BS + C14Ac + cosurfactant is due to the formation of mixed adsorption layers in which the incorporated, shorter-chain molecules reduce the cohesion between the adsorbed molecules in the condensed adsorption layer. The decrease in the surface modulus for BS + C14Ac is more pronounced when C10 additives are used, as compared to C8 additives, which might be explained with the incorporation of more C10 molecules (which are more surface active) in the mixed adsorption layer, as compared to C8 molecules. No significant difference between fatty acids and fatty alcohols of the same chain-length is observed.

From these measurements we conclude that the chosen surfactant mixtures cover a relatively wide range of dynamic surface tensions, between 35 and 44 mN/m (as measured at ca. 100 ms of surface age),

and surface dilatational moduli, between 1 and 300 mN/m. Therefore, we can study systematically the effect of these surface properties on the foaming properties of the respective surfactant solutions.

3.2. Effect of the operating conditions on the foaming process

We start with the effect of the volume of the surfactant solution, used for foam generation. In Fig. 4 we show illustrative results for this effect, obtained with solution of BS + 30 wt% glycerol. One sees from Fig. 4A that the larger solution volumes lead to larger amount of trapped air and faster rate of foam generation.

When the same data are replotted in terms of trapped air volume fraction versus time, Fig. 4B, it is seen that the foaming process stops at the same air volume fraction for all three solution volumes studied. The mean bubble size in the formed foams is also very similar, which means that the final outcome of the foaming process does not depend on the volume of the initial surfactant solution. This is an important experimental fact which is explained in Section 3.6 below, after presenting all experimental results.

For the two larger solution volumes, 300 and 500 mL, the kinetics of foam generation also falls on the same curve after replotting the data in the form air volume fraction vs. time, see Fig. 4B. On the other hand, the data for the smallest solution volume, 150 mL, are different with the presence of a relatively long induction period of ca. 200 s before the process of rapid foam generation is observed, Fig. 4B. The most probable explanation for the observed induction period in this system is the inhomogeneous shear rate in the bowl, as shown in Ref. [29]. At the smallest solution volume, the upper surface of the initial solution is below the threshold vertical position (*z*-position), above which the shear rate becomes significantly higher as compared to the lower positions, cf. with Fig. 7 in Ref. [29]. Therefore the initial induction period observed with smaller solution volumes is due to a process of relatively slow accumulation of bubbles on the solution surface until it rises to reach the *z*-level, at which the shear rate is sufficiently high and the stirring is more efficient. Afterwards, the foaminess increases rapidly.

From these experiments we conclude that, for a given surfactant solution, the foaming process stops when foams with given air volume fraction and mean bubble size are formed, even when surfactant solutions with different initial volumes are used. Also, the intensive process of foaming starts above a given shear rate, applied to the surfactant solution.

The effect of shear rate on the foaming process was studied systematically with BS + 40 wt% glycerol, Fig. 5. Three regions in the curves volume of trapped air vs. time, V_A vs. *t*, are observed: (1) Induction period–the air entrapment is very slow until a critical amount of bubbles is accumulated on the solution surface to reach the level where the shear rate is high enough to induce fast air entrapment. To
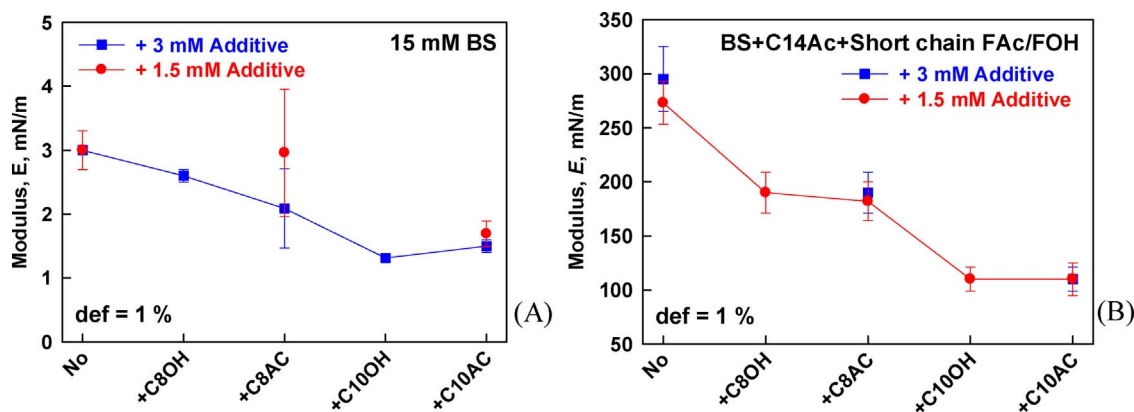
Fig. 3. Surface moduli of solutions of (A) BS + Additives and (B) BS + C14Ac + additives at two different concentrations of additives of 1.5 mM (red circles) and 3 mM (blue squares). Modulus are measured at $T = 20$ °C and frequency of oscillation of 2 Hz. The amplitude of deformation is 1%. (For interpretation of the references to colour in this figure legend, the reader is referred to the web version of this article.)

characterize this stage we determined the induction time, t_{IND}, which is defined as the time required for reaching an air volume fraction of 0.66; (2) Fast foam generation where the entrapped air increases almost linearly with time. For characterization of this stage we determine the rate of increase of the foam volume, dV/dt; (3) Plateau region in which the volume of trapped air remains constant. The final foams are characterized by their air volume fraction, Φ, mean volume-surface bubble radius, R_{32}, and their rheological properties.

As seen from Fig. 5B, the induction time decreases by more than 10 times (450 vs. 38 s) upon a 2-fold increase of the shear rate during foaming (1.5 vs. 3 rps). This decrease in t_{IND} is accompanied with a 30 times increase of the rate of foam generation during the second stage (2.5 vs. 86 mL/s) at higher share rate. Thus, the higher shear rate facilitates in a non-linear manner both the air entrapment during the induction period and the foam build up.

The final outcome of foaming also depends on the hydrodynamic conditions. The final foam volume is 3 times higher for foams prepared at 3 rps, as compared to those prepared at 1.5 rps. Importantly, we found that the mean bubble size in the final foams depends very weakly on the shear rate during foam generation − R_{32} decreases from 235 to 210 μm upon a 2-fold increase of the shear rate, see Fig. 5C. Therefore, these two effects are also non-linear, but the effect of rotation speed on foam volume is very significant, whereas the effect on bubble size is rather small.

From this series of experiments we conclude that the duration of the induction period decreases by 10 times, the rate of fast foam build-up increases by 30 times, and the final volume of trapped air increases by 3 times upon a 2-fold increase of the shear rate, whereas the mean bubble size in the final foams is almost the same for all shear rates studied.

3.3. Effect of the solution surface properties on the foaming process

The effect of dynamic surface tension (DST) was studied by performing experiments with BS + cosurfactant solutions with different DST profiles, cf. Fig. 2A. The kinetics of air entrapment in these solutions is compared in Fig. 6A. The presence of short-chain additives slightly decreases the induction time from 95 s down to 70 s and increases by 30% the rate of foam generation in the second stage, from 7 to 10 mL/s. However, the presence of these additives practically does not affect the properties of the final foams. All final foams have air volume fraction ≈ 0.95 and mean bubble size, $R_{32} \approx 275 \pm 15$ μm for BS and BS + FOH, and ≈ 240 ± 15 μm for BS + FAc. Therefore, the faster adsorption on the bubble surface facilities the air entrapment during the first and the second stages of foam generation, but it does not affect significantly the final outcome of the foaming process.

To clarify the effect of surface modulus on the foaming process, we performed experiments with BS + C14Ac and BS + C14Ac + FAc or FOH solutions. Among these solutions, the surface modulus varies between ca. 100 and 300 mN/m, see Fig. 3B above.

From the results presented in Fig. 7A one sees that the addition of C14Ac to BS solution leads to a very significant change in the main properties of the final foam. The foam generation during the first and second stages appears very similar for BS and BS + C14Ac, but the air entrapment stops at much earlier moment, at around 2-times lower foam volume in the presence of C14Ac, as compared to the BS solution. Furthermore, the final foam generated from BS + C14Ac solution contains around two times smaller in radius bubbles, see Fig. 7B. Therefore, we conclude that the formation of condensed adsorption layer on the bubble surfaces, in the presence of C14Ac, leads to much
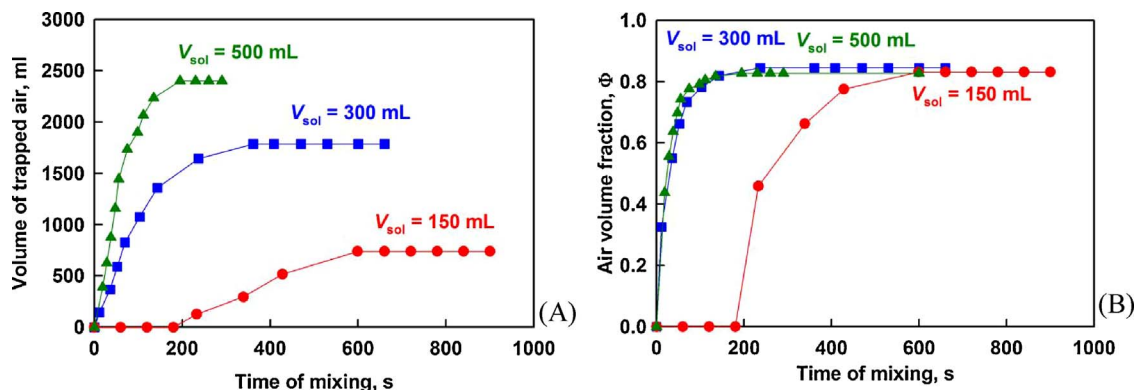

Fig. 4. Effect of the solution volume on the kinetics of foam generation. (A) Volume of trapped air and (B) Air volume fraction vs. time of mixing at different initial volumes of the foaming solution: 500 mL (green triangles); 300 mL (blue squares); 150 mL (red circles). Foaming solution: BS (0.5 wt.%) + glycerol (30 wt.%). Rate of rotation: 1.5 rps. (For interpretation of the references to colour in this figure legend, the reader is referred to the web version of this article.)
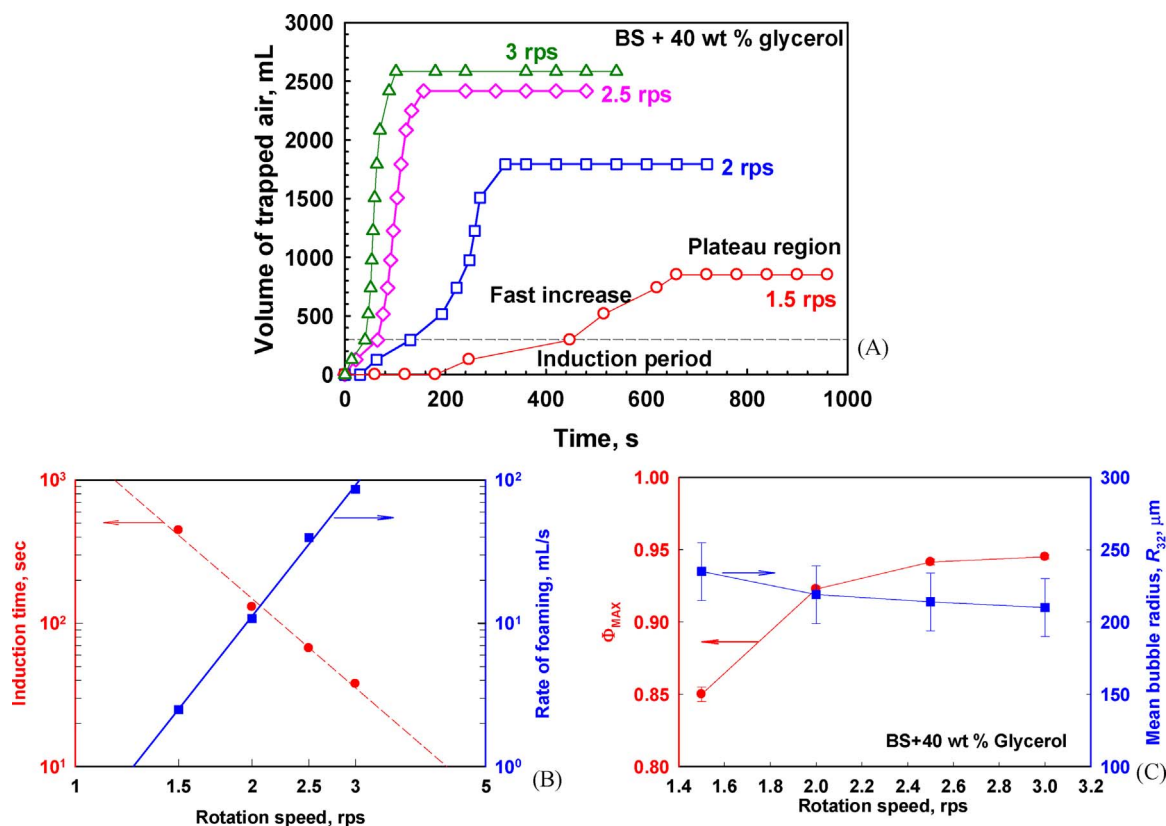
Fig. 5. (A) Volume of trapped air vs. mixing time at different rotation speeds, as described in the figure. (B) Induction time (red circles) associated to the left axis and rate of foaming (blue squares) associated with the right axis, as functions of the rotation speed of the mixing tool; (C) Maximum air volume fraction in the plateau region (red circles) associated with the left axis and mean bubble radius (blue points) associated with the right axis vs. the rotation speed. Experimental conditions: 150 mL foaming solution of 0.5 wt% BS + 40 wt% glycerol, $T = 20\,°C$. (For interpretation of the references to colour in this figure legend, the reader is referred to the web version of this article.)

faster bubble breakage to smaller bubbles which, in its turn, reduces the final foam volume.

The addition of short-chain additives to BS + C14Ac solution decreases the induction time and increases the rate of foaming in the second stage, due to the faster surfactant adsorption. Nevertheless, the final foam has properties resembling those of the BS + C14Ac solution. In particular, the mean bubble size in the final foams is small, see Fig. 7B, because the surface modulus of all these solutions is > 100 mN/m, see Fig. 3B above.

From these experiments we conclude that the additives which decrease the dynamic surface tension do increase the rate of foam generation and shorten slightly the induction time. However, they do not change the air volume fraction and the mean bubble size in the final

foams. In contrast, C14Ac, which forms condensed adsorption layer on the bubble surface and increases the surface viscoelasticity, does not affect significantly the rate of foam generation (because it does not affect significantly the DST) but changes very strongly the final outcome of the foaming process–it leads to much smaller bubbles and lower air volume fraction. Mixtures of short-chain additives and C14Ac combine both effects as they lead to faster air entrapment and smaller bubbles in the final foams. Note that the volume of the foam, produced from 150 mL surfactant solution, falls in the range of 1500–2500 mL which corresponds to air volume fraction, Φ, between 90 and 94 vol%. This means that the foaming solution, 6–10 vol.%, was entirely incorporated inside the sheared foam (i.e. exhausted).
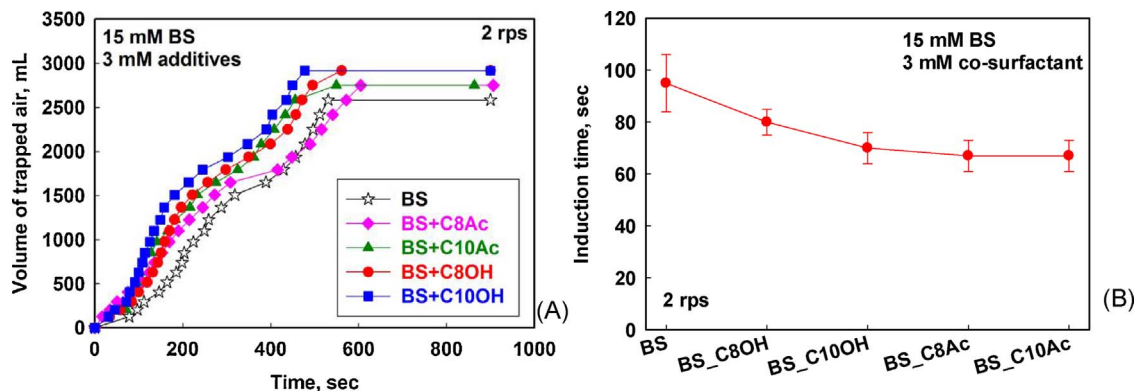

Fig. 6. (A) Volume of trapped air vs. mixing time for foams prepared from various surfactant solutions, as described in the figure. (B) Induction time for the systems studied. Volume of the foaming solution: 150 mL. $T = 20\,°C$. All solutions contain 15 mM BS + 3 mM additive. Foaming is performed at 2 rps.
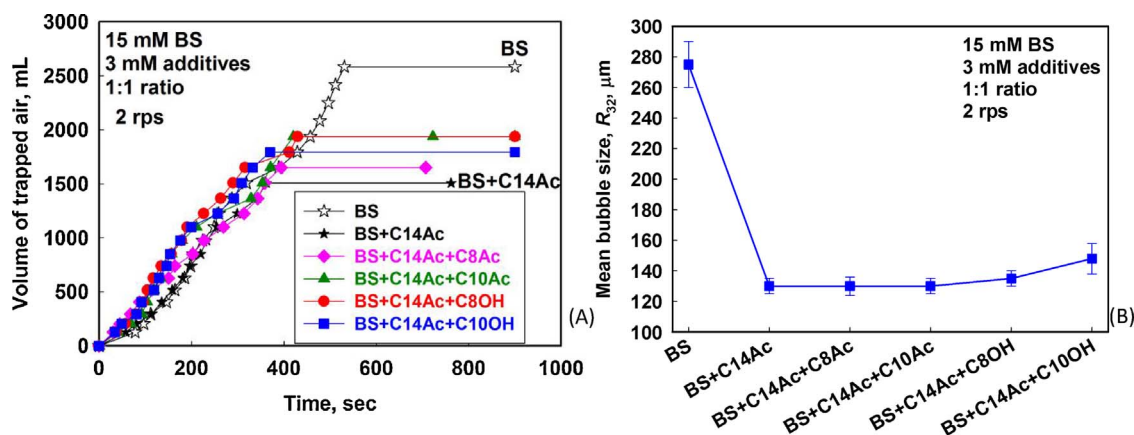
Fig. 7. (A) Volume of trapped air vs. mixing time for foams prepared from various surfactant solutions, as described in the figure. (B) Mean bubble size in the final foam. Volume of the foaming solution: 150 mL. $T = 20\,°C$. All solutions contain 15 mM BS + 3 mM additive. Foaming is performed at 2 rps.

3.4. Effect of solution viscosity

Experiments at different glycerol concentrations, with both BS and BS + C14Ac solutions, were performed to clarify the effect of solution viscosity on the foaming process. The obtained results for the final foam volume and the mean bubble size are shown in Fig. 8. For both types of solutions, with high and low surface moduli, the increase of solution viscosity leads to a very significant reduction in the volume of trapped air, accompanied with a significant decrease in the size of the formed bubbles, see Fig. 8B. Thus, from the solution with the highest viscosity, 550 mPa.s, we obtained foams with air volume fraction of $\approx 78\%$ and mean bubble radius of 15–20 μm.

The effects of solution viscosity on the mean bubble size and on the volume of trapped air appear to be strongly correlated–see Sections 3.5 and 3.6 for explanation, further discussion and quantitative description of this correlation.

3.5. Optical observations and mechanism of air entrapment

The experimental results presented so far show that the final outcome of foam generation depends very significantly on the viscosity and on the surface dilatational modulus of the surfactant solutions, whereas the dynamic surface tension has negligible effect. On the other hand, the dynamic surface tension affects to some extend the rate of foaming by decreasing the induction time and increasing the rate of air entrapment in the second stage of the foaming process. To clarify the mechanism of air entrapment which should explain these trends, we performed optical observations of the foaming process with a high speed video-camera.

The optical observations revealed that the rotation of the mixer tool generates waves with relatively large amplitude on the solution surface during the induction period and on the foam surface during the second stage of foaming (fast increase of V_A). The metal rods of the tool entrain foam and trap relatively large pockets of air during these two stages. This process is illustrated in Fig. 9. Fig. 9A and B show the formation of a large cavity on the foam surface, which is eventually covered by a foam layer (Fig. 9C) to form a large air pocket. The same process is depicted schematically in Fig. 9D–F. In parallel, the trapped air pockets are gradually broken down to much smaller bubbles inside the sheared foam.

These observations clarify the main mechanisms, governing the observed experimental trends. The air entrapment leads to increase of the air volume fraction in the foam, simultaneous decrease in the bubble size due to multiple bubble breakup events in the sheared foam, and to related increase in the viscoelastic response of the foam. As a consequence, at a certain critical value of the foam shear stress, τ_{CR}, the power of mixing (at the respective rotation speed) becomes unable to generate waves of sufficiently large amplitude on the foam surface. There are still corrugations (waves) on the foam surface, created by the rotating tool, but they have relatively low amplitude and are unable to trap air (see Fig. 10).

To verify this explanation, we measured the rheological properties of the foams, formed at a given shear rate from solutions with very different surface and bulk properties. The obtained results from these measurements are compared in Fig. 11. One sees from Fig. 11B that the dependence of the dimensionless shear stress on the shear rate is rather similar for all these foams, in the range of shear rates which are relevant to the foaming process (40–90 s^{-1}). The latter result is far from trivial,
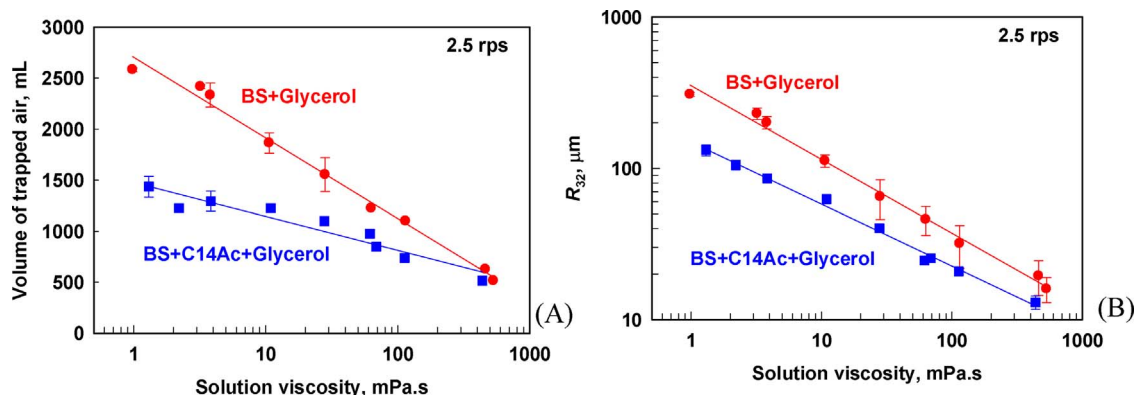

Fig. 8. (A) Maximum volume of trapped air and (B) Mean bubble radius as a function of solution viscosity varied by addition of glycerol. Solution: BS (red circles); BS + C14Ac (blue squares). Volume of the foaming solution: 150 mL $T = 20\,°C$. Rate of mixing: 2.5 rps. (For interpretation of the references to colour in this figure legend, the reader is referred to the web version of this article.)
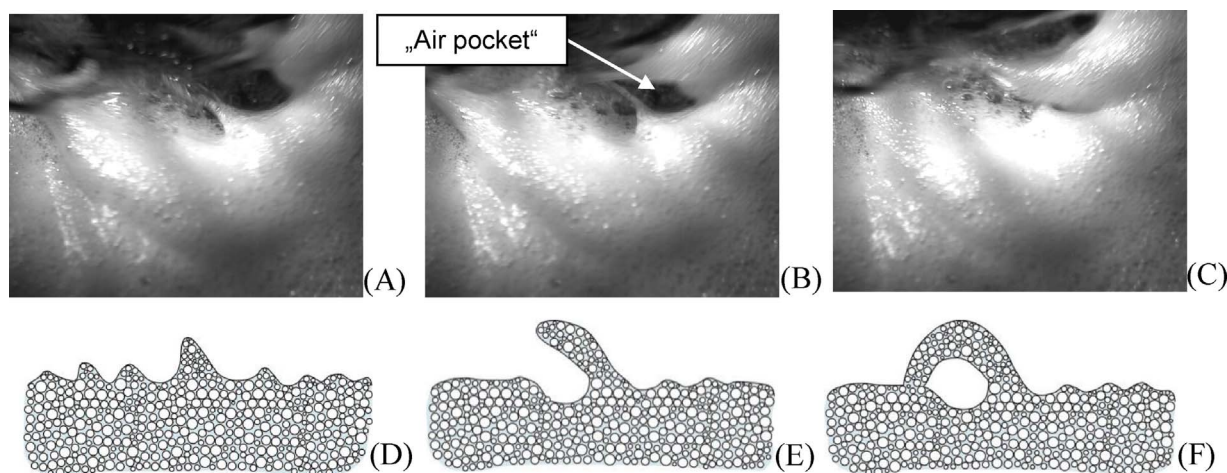
Fig. 9. Pictures of a bubble entrapment event, observed with a high-speed video camera. (A) A cavity is formed on the surface of sheared foam; (B) Large wave on the foam surface, created by the rotating mixing tool, covers the cavity; (C) Thus an air pocket is trapped in the foam. (D-F) Schematic presentation of the main consecutive steps in the air entrapment event.

as the data shown in Fig. 11 are obtained with foams which vary significantly in their air volume fraction, mean bubble size, surface viscoelasticity and solution viscosity (that is why the dimensional stress, shown in Fig. 11A, is different for all these systems). Therefore, a strong correlation between all these properties must exist to result in final foams with very similar dimensionless rheological properties, in the range of shear rates representing the foaming process.

As the shear rate in the foaming experiments vary in a narrow range (40–90 s^{-1}), the results shown in Fig. 11B mean also that the critical shear stress, leading to damped air entrapment, is similar for all these systems when presented in dimensionless form, $\tilde{\tau}_{CR} \equiv \tau_C R_{32}/\sigma \approx 0.25 \pm 0.05$. In other words, the amplitude of the formed waves on the foam surface is controlled by the dimensionless shear stress, rather than by its dimensional counterpart.

This general result can be explained in the following way. As already described, the processes of air entrapment and bubble breakup occur in parallel during the second stage of the foaming, in which the foam generation is most intensive. As a result, the air volume fraction increases and the average bubble size decreases, thus leading to a rapid increase of the foam viscoelasticity which eventually damps the surface waves and stops the further increase of the foam volume when the foam shear stress approaches $\tilde{\tau}_{CR}$.

For the solutions with the same viscosity, but having different surface dilatational moduli, the initial period of air entrapment is similar, while the bubble breakup is much faster for the solutions with high surface modulus as shown in our previous study [36]. Therefore, for these solutions, the initial fast process of air entrapment is accompanied with a highly efficient bubble breakup and related increase of foam viscoelasticity. As a result, the foam generation stops at lower air

volume fraction and the final foams contain smaller bubbles. Similarly, the increase of the solution viscosity at given surface properties leads to more difficult air entrapment in the initial stages and the critical foam stress which damps the air entrapment is reached faster − again foams with less volume and smaller bubbles are formed.

This mechanism of foam generation explains also the observed effect of the shear rate on the kinetics of foam generation. On one hand, when the rotation rate of the tool is higher, more surface waves per unit time are generated and the air entrapment events are more frequent–this results in shorter induction time and faster foaming, see Fig. 5C. The effect is strongly non-linear because not only the shear rate *per se* is higher, but also the foam effective viscosity is lower at the higher shear rates. As a result, the foam is more deformable and the air entrapment is strongly facilitated.

Let us emphasize here that the bubble size and air volume fraction in the studied foams are not affected by the possible bubble coalescence, due to the appropriate choice of the foamed surfactant solutions. The surfactants used in the current study and their concentration (15 mM) are chosen in a way which ensures very stable foams with respect to bubble coalescence. The main surfactants, SLES and CAPB, are among the best foam stabilizers known and their concentration is much higher than the CMC ≈ 0.5 mM. The possible depletion of surfactant molecules, due to their adsorption on the newly formed bubble surface during foaming, is negligible, as one could show by simple estimates.

The assumption for negligible role of bubble coalescence in our study is directly supported by two experimental observations. The high-speed camera observations showed that the increase in the foam volume stops when no further air is entrapped during shearing. Hence, the
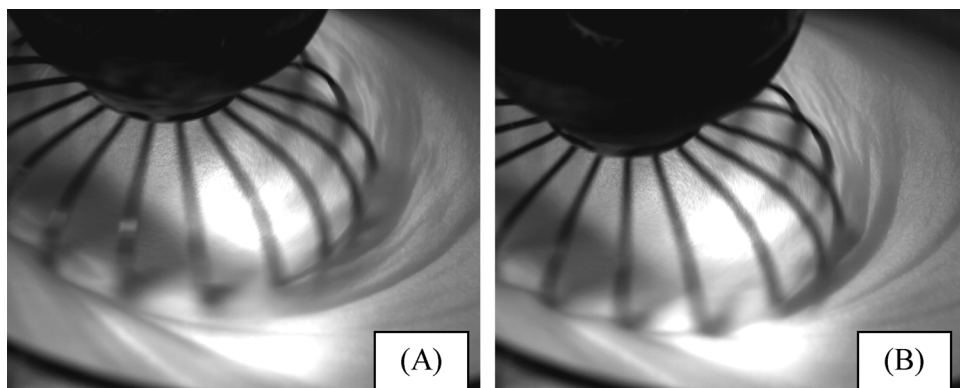

Fig. 10. Consecutive images of the surface of the foam during mixing in the plateau region when the foam volume remains constant. Due to the significant viscoelasticity of the foam, the hydrodynamic waves on the foam surface have small amplitude, and there is no further air entrapment.
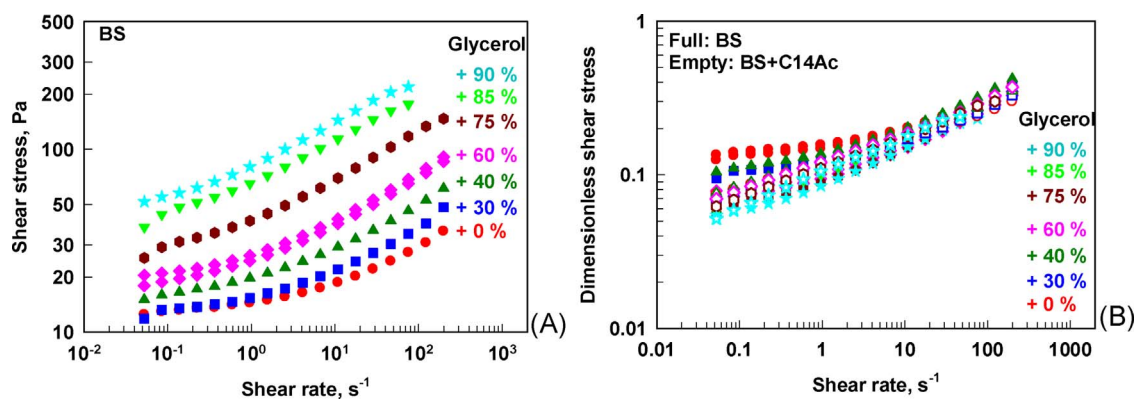
Fig. 11. (A) Dimensional and (B) Dimensionless shear stress, $\tilde{\tau} \equiv \tau R_{32}/\sigma$, vs. shear rate of foams stabilized by different surfactant formulations, containing different levels of glycerol, as shown in the figures. All these foams are prepared at 2 rps rotation speed and taken from the final plateau region in the foam evolution. Volume of the foaming solution: 150 mL.

final foam volume in our experiments is not determined by equal rates of simultaneous air entrapment into the foam and air release from the foam (due to bubble coalescence). This conclusion is supported also by the second observation that the foam height remained constant for long periods (> 1 h) after stopping the mixing rotor. In these aspects, our experiments are in sharp contrast with the experiments, performed by other authors with unstable foams, see e.g. the review Ref. [38]. In the latter systems, a steady-state foam column is formed as a result of dynamic equilibrium between the entrapped and the released air (due to bubble coalescence). Accordingly, in the latter experiments one observes a rapid decrease of the foam volume immediately after stopping the air entrapment, a phenomenon which has never been observed in our experiments.

The most important conclusions from the current section can be summarized as follows. During shearing, waves with large amplitude are generated on the foam surface. When the amplitude of these waves is sufficiently large, air pockets (large bubbles) are trapped which leads to larger foam volume. The trapped large bubbles are gradually broken down into much smaller bubbles and this process is much faster at higher surface modulus and higher viscosity of the foaming solutions. Both the air entrapment and bubble breakup result in a significant increase of the foam shear stress with time. When a given critical value of the dimensionless foam stress is reached, $\tilde{\tau}_{CR} \approx 0.25$, any further air entrapment is impeded, as the amplitude of the waves on the foam surface becomes very small. The dimensionless stress is important because both sub-processes, the surface agitation by the rotating tool (wave generation) and the damping of the generated surface waves, are more pronounced at higher foam viscoelasticity. The possible effects of bubble coalescence are negligible in our experiments, due to the appropriate choice of foamed surfactant solutions.

This mechanism explains qualitatively all observed effects on the kinetics of foam generation and on the properties of the final foam.

3.6. Properties of the final foams

For given surfactant solution, the foam viscoelasticity depends strongly on both the mean bubble size, R_{32}, and the bubble volume fraction, Φ. During foaming, these two quantities evolve in the coupled processes of air entrapment and bubble breakup. To clarify the relations between the final outcome of the foaming process, the material properties of the initial solution and the operating conditions during foaming, we searched for quantitative correlations between these characteristics. The systems of high and low surface modulus are considered separately, as the experimental data show that these are two different regimes which obey different functional dependences.

We consider first the solutions with low surface modulus which do not contain C14Ac. Interpolation of the obtained experimental data (Figs. 4–8) by power-law functions showed that:

$$R_{32} \approx A_1 \eta_C^{-1/2} \dot{\gamma}^{-0.15} \tag{2}$$

$$\Phi_L \approx A_2 \eta_C^{1/4} \dot{\gamma}^{-3/2} \tag{3}$$

where $\Phi_L = (1-\Phi)$ is the liquid volume fraction in the final foam, and A_1 and A_2 are dimensional constants. Note that these relations cannot be presented as direct dependences on the capillary number, $Ca = \eta_C \dot{\gamma} R_{32}/\sigma$, which confirms our statement that the final foam is obtained as a result of complex interplay between the coupled kinetic processes of air entrapment and bubble breakup in the sheared foams.

Since the values of R_{32} and Φ_L in the final foam are interrelated, we searched for a single equation which could describe all experimental data obtained at different viscosities and different shear rates. One cannot find such a relation just by combining Eqs. (2) and (3) because the value of the constant A_1 in Eq. (2) corresponds to different values of Φ_L and the value of the constant A_2 in Eq. (3) corresponds to different values of R_{32}. In other words, there are implicit hidden dependences on Φ_L and R_{32} in Eqs. (2) and (3).

Therefore, we searched for a combination of R_{32} and Φ_L which could be described by a single power-law equation. We found that all experimental data for low surface modulus systems are described very well, with a very high correlation coefficient $R^2 > 0.99$, by the simple power-law relation (see Fig. 12A):

$$\frac{R_{32}}{\Phi_L^{1/2}} = A_3 \left(\frac{\dot{\gamma}}{\eta_C} \right)^{2/3} \tag{4}$$

Similar analysis for the solutions with high surface modulus, containing C14Ac, revealed that all experimental data could be described with the following power-law functions, see Fig. 12B:

$$R_{32} \approx A_4 \eta_C^{-0.42} \dot{\gamma}^{-2/3} \tag{5}$$

$$\Phi_L \approx A_5 \eta_C^{0.15} \dot{\gamma}^{-1/2} \tag{6}$$

and the respective counterpart of Eq. (4):

$$\frac{R_{32}}{\Phi_L^{1/2}} = A_6 (\dot{\gamma}\eta_C)^{-2/5} \tag{7}$$

Note that the functional dependences for the systems with high and low surface moduli are rather different which confirms our statement that these are two different regimes of foaming (cf. Eq. (2) with Eq. (5), Eq. (3) with eq. (6), and Eq. (4) with Eq. (7)). Similar qualitative differences between the systems of high and low surface moduli have been already reported for the foam rheological properties [39] and for the bubble breakup in sheared foams [40]. The transitional value of the surface modulus which separates these two regimes was reported to be $\approx 100 \pm 25$ mN/m [31] and the current results comply with this value. Note that in the above analysis, the surface modulus is used only to discriminate between the two regimes of foam dynamics,
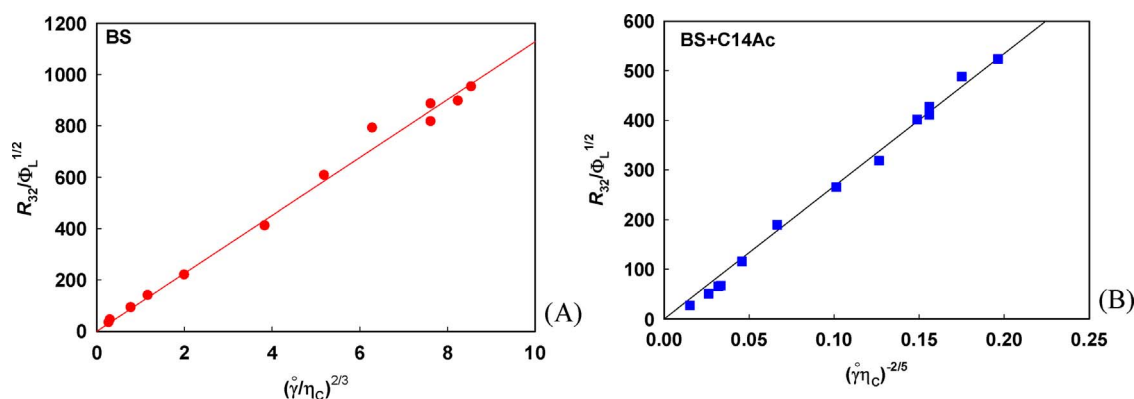
Fig. 12. Dependences of the mean bubble size, R_{32}, and liquid volume fraction, Φ_L, in the final foam on the viscosity of the foaming solution, η_C, and the shear rate during foaming, $\dot{\gamma}$, for solutions with (A) low surface modulus, and (B) High surface modulus. Volume of the foaming solution: 150 mL.

corresponding to high and to low surface moduli, respectively. The specific value of the surface modulus does not appear in the final equations. Additional explanations about the role of surface modulus in foam dynamics are presented in [30,39].

The above analysis revealed explicit relations between the characteristic (maximum) shear rate in the mixer and the main properties of the formed foams, Eqs. (2)–(7). One may expect that foaming experiments performed with other rotational mixers of similar type will result in similar functional dependences with, possibly, somewhat different numerical pre-factors. For each specific foaming device one should determine and use its characteristic shear rate for the data analysis, because this is the rate responsible for the bubble breakup and for the air entrapment (through the surface wave formation).

4. Main results and conclusions

In the current study we investigate the process of foam generation in a planetary mixer. We have evaluated the effects of the hydrodynamic conditions during foaming (rate of mixing) and of the material properties of the foamed solutions (viscosity, dynamic surface tension and dilatational surface modulus) on the rate of foam generation and on the final foam properties–air volume fraction, Φ, and mean bubble radius, R_{32}. The most important results and conclusions can be summarized as follows:

- There are 3 main periods in the process of foam generation. The first one is the so-called "induction period" in which a very slow increase in the volume of trapped air is observed. During the second period, the foam volume increases rapidly. Eventually, the foam volume reaches a constant value (plateau) in the third period.
- The direct observations of the foaming process with a high-speed video camera showed that the mixing tool generates waves on the surface of the foam which lead to entrapment of air pockets inside the foam. These air pockets (big bubbles) are broken-down to smaller bubbles under the action of the shear stress in the agitated foam. The processes of air entrapment and bubble breakup occur simultaneously, although with different relative intensity in the various stages of the foaming process and for different solutions. The net result is that the shear stress in the sheared foam increases rapidly during the second stage of the foaming process.
- The key parameter which controls the air volume fraction and the bubble size in the final foam is the dimensionless shear stress of the foam. This characteristic was very similar for all final foams studied, at the shear rates relevant to foaming, irrespectively of the solution used to generate these foams. In other words the air entrapment stops when a given dimensionless critical shear stress, $\tilde{\tau}_C \approx 0.25 \pm 0.05$, is reached. In solutions with higher viscosity and/or surface modulus, $\tilde{\tau}_C$ is reached at lower air volume fraction,

due to the faster bubble breakage as compared to air entrapment. That is why, both the volume of trapped air and the bubble size decrease strongly upon increase of solution viscosity and/or surface modulus.
- Simple power-law functions are shown to describe very well the observed relations between the solution properties, the shear rate and the final foam properties.

These conclusions elucidate the complexity of the foaming process and provide important clues for its optimization under conditions relevant to practice. The obtained experimental data and the observed general trends are appropriate starting point for detailed theoretical modelling which should describe the complex interplay between the kinetic processes of air entrapment and bubble breakup under conditions, representing the foaming process. The used approach and the obtained conclusions could help also in the analysis of other foaming techniques in which the air entrapment occurs via mechanical agitation of free foam surface, such as the Ross-Miles test and Bartsch method. The studied phenomena are mechanistically related also to the effect of damping of liquid sloshing by thin foam layers, described in refs. [41]. The conditions of the performed experiments (selected surfactants and their concentrations) were chosen to avoid the possible effects of bubble coalescence. The latter process could be important at lower surfactant concentrations and/or for other surfactants, and would add further complexity in the studied phenomena.

Note that the alternative foaming tests which allow for free simultaneous variation of the foam volume and bubble breakup, such as the Ross-Miles test, Bartsch test and automated shake test, all have less-characterized dynamic zone, in which one cannot determine a well-defined maximum shear rate, as in the case of the planetary mixer used here. Therefore, this type of mixers seems best suited for the purpose of our study, as they have clearly-defined geometry and maximum shear rate (see Supplementary Materials section). In addition, such mixers are widely used in several areas and, hence, the obtained results are of practical relevance as well.

Acknowledgements

Appendix A. Supplementary data

Supplementary data associated with this article can be found, in the online version, at https://doi.org/10.1016/j.colsurfa.2017.12.006.

References

[2] I. Cantat, et al., Foams: Structure and Dynamics, Oxford University Press, UK, 2013.

[3] Foams, R. K. Prud'homme, S.A. Kahn (Eds.), Theory, Measurements and Application, Marcel Dekker New York, USA, 1996.

[4] D. Exerowa, P.M. Kruglyakov, Foams and Foam Films: Theory Experiment, Application, Elsevier, Amsterdam, 1998.

[5] S.A. Koehler, S. Hilgenfeldt, H.A. Stone, A generalized view of foam drainage: experiment and theory, Langmuir 16 (2000) 6327.

[6] O. Pitois, C. Fritz, M. Vignes-Adler, Liquid drainage through aqueous foam: study of the flow on the bubble scale, J. Colloid Interface Sci 282 (2005) 458.

[7] A. Saint-Jalmes, Physical chemistry in foam drainage and coarsening, Soft Matter. 2 (2005) 836.

[8] J. Lambert, I. Cantat, R. Delannay, R. Mokso, P. Cloetens, J.A. Glazier, F. Graner, Experimental growth law for bubbles in a wet 3D liquid foam, Phys. Rev. Lett. 99 (2007) 058304.

[9] S.M. Bhavaraju, T.W.F. Russell, H.W. Blanch, The design of gas sparged devices for viscous liquid systems, AIChE J. 24 (1978) 454.

[10] J.F. Walter, H.W. Blanch, Bubble break-up in gas-liquid bioreactors: break-up in turbulent flows, Chem. Eng. J. 32 (1986) B7.

[11] C. Martinez-Bazan, J.L. Montanes, J.C. Lasheras, On the breakup of an air bubble injected into a fully developed turbulent flow. Part 1. Breakup frequency, J. Fluid Mech. 401 (1999) 157.

[12] C. Martinez-Bazan, J.L. Montanes, J.C. Lasheras, On the breakup of an air bubble injected into a fully developed turbulent flow. Part 2. Size PDF of resulting daughter bubbles, J. Fluid Mech. 401 (1999) 183.

[13] W. Drenckhan-Andreatta, A. Saint-Jalmes, The science of foaming, Adv. Colloid Interface Sci. 222 (2015) 228–259, http://dx.doi.org/10.1016/j.cis.2015.04.001.

[14] J.J. Bikerman, Methods of Measuring Foaminess In Foams: Theory and Industrial Applications, Reinhold, New York, 1953, pp. 27–49.

[15] J.J. Bikerman, Measurement of Foaminess In Foams, Springer-Verlag, New York, 1973, pp. 65–97.

[16] P.R. Garrett, Recent developments in the understanding of foam generation and stability, Chem. Eng. Sci. 48 (2) (1993) 367–392.

[17] A. Patist, S.G. Oh, R. Leung, D.O. Shah, Kinetics of micellization: its significance to technological processes, Colloids Surf. A 176 (2001) 3.

[18] A. Patist, T. Axelberd, D.O. Shah, Effect of long chain alcohols on micellar relaxation time and foaming properties of sodium dodecyl sulfate solutions, J. Colloid Interface Sci. 208 (1998) 259.

[19] S. Pandey, R.P. Bagwe, D.O. Shah, Effect of counterions on surface and foaming properties of dodecyl sulfate, J. Colloid Interface Sci. 267 (2003) 160.

[20] K.G. Marinova, E.S. Basheva, B. Nenova, M. Temelska, A.Y. Mirarefi, B. Campbell, I.B. Ivanov, Physico-chemical factors controlling the foamability and foam stability of milk proteins: sodium caseinate and whey protein concentrates, Food Hydrocolloids 23 (2009) 1864.

[21] X.-C. Wang, L. Zhang, Q.-T. Gong, L. Wang, L. Zhang, L. Luo, Z.-Q. Li, S. Zhao, J.-Y. Yu, A study of dynamic interfacial properties as related to foaming properties of sodium 2,5-dialkyl benzene sulfonates, J. Dispersion Sci. Techn. 30 (2009) 346.

[22] X.-C. Wang, L. Zhang, Q.-T. Gong, L. Zhang, L. Luo, Z.-Q. Li, S. Zhao, J.-Y. Yu, Study on foaming properties and dynamic surface tension of sodium branched-alkyl benzene sulfonates, J. Dispersion Sci. Techn. 30 (2009) 137.

[23] X.-W. Song, L. Zhang, X.-C. Wang, L. Zhang, S. Zhao, J.-Y. Yu, Study on foaming properties of polyoxyethylene alkyl ether carboxylic salts with different structures, J. Dispersion Sci. Techn. 32 (2011) 247.

[24] M.A. Bos, B. Dunnewind, T. Van Vliet, Foams and surface rheological properties of β-casein, gliadin and glycinin, Colloids Surf. B 31 (2003) 95.

[25] C.D. Dushkin, T.L. Stoichev, T.S. Horozov, A. Mehreteab, G. Broze, Dynamics of foams of ethoxylated ionic surfactant in the presence of micelles and multivalent ions, Colloid Polym. Sci. 281 (2003) 130.

[26] A. Pinazo, L. Pérez, M.R. Infante, E. Franses, I: Relation of foam stability to solution and surface properties of gemini cationic surfactants derived from arginine, Colloids Surf. A 189 (2001) 225.

[27] T. Tamura, Y. Kaneko, M.J. Ohyama, Dynamic surface tension and foaming properties of aqueous polyoxyethylene *n*-dodecyl ether solutions, Colloid Interface Sci. 173 (1995) 493.

[28] M.J.P. Hiseman, B.F.C. Laurent, J. Bridgwater, D.I. Wilson, D.J. Parker, N. North, D.R. Merrifield, Granular flow in a planetary mixer, Chem. Eng. Res. Des. 80 (2002) 432–440.

[29] A.K.S. Chesterton, G.D. Moggridge, P.A. Sadd, D.I. Wilson, Modelling of shear rate distribution in two planetary mixtures for studying development of cake batter structure, J. Food Eng. 105 (2011) 343–350.

[30] K. Golemanov, N.D. Denkov, S. Tcholakova, M. Vethamuthu, A. Lips, Surfactant mixtures for control of bubble surface mobility in foam studies, Langmuir 24 (2008) 9956.

[31] Z. Mitrinova, S. Tcholakova, K. Golemanov, N. Denkov, M. Vethamuthu, K.P. Ananthapadmanabhan, Surface and foam properties of SLES + CAPB + fatty acid mixtures: effect of pH for C12–C16 acids, Colloid Surf. A 438 (2013) 186.

[32] Z. Mitrinova, S. Tcholakova, J. Popova, N. Denkov, B. Dasgupta, K.P. Ananthapadmanabhan, Efficient control of the rheological and surface properties of surfactant solutions containing C8-C18 fatty acids as cosurfactants, Langmuir 29 (2013) 8255–8265.

[33] S.C. Russev, N. Alexandrov, K.G. Marinova, K.D. Danov, N.D. Denkov, L. Lyutov, V. Vulchev, C. Bilke-Krause, Instrument and methods for surface dilatational rheology measurements, Rev. Sci. Instrum. 79 (2008) 1864.

[34] P.R. Garrett, J.D. Hines, S.C. Joyce, P.T. Whittal, Report prepared for Unilever R&D, Port Sunlight, (1993).

[35] S. Mukherjee, H. Wiedersich, Morphological and Viscoelastic properties of dense foams generated from skin cleansing bars, Colloids Surf. A 95 (1995) 159.

[36] Rasband W.S., J. Image, U. S. National Institutes of Health Bethesda, Maryland, USA, http://rsb.info.nih.gov/ij, 1997–2015.

[37] N.D. Denkov, V. Subramanian, D. Gurovich, A. Lips, Wall slip and viscous dissipation in sheared foams: effect of surface mobility, Colloids Surf. A 263 (2005) 129.

[38] J. Wang, A.V. Nguyen, S. Farrokhpay, A critical review of the growth, drainage and collapse of foams, Adv. Colloid Interface Sci. 228 (2016) 55–70, http://dx.doi.org/10.1016/j.cis.2015.11.009.

[39] N. Denkov, S. Tcholakova, K. Golemanov, K.P. Ananthpadmanabhan, A. Lips, Role of surfactant type and bubble surface mobility in foam rheology, Soft Matter. 7 (2009) 3389–3408.

[40] K. Golemanov, S. Tcholakova, N.D. Denkov, K.P. Ananthpadmanabhan, A. Lips, Bubble/drop breakup in steadily sheared foams and concentrated emulsions, Phys. Rev. E 78 (2008) 051405.

[41] A. Sauret, F. Boulogne, J. Cappello, E. Dressaire, H.A. Stone, Damping of liquid sloshing by foams, Phys. Fluids 27 (2015) (022103-1-022103-15).